

# Lubricating Grease Flow in a Double Restriction Seal Geometry: A Computational Fluid Dynamics Approach

Lars G. Westerberg<sup>1</sup>  · Chiranjit Sarkar<sup>1,3</sup> · Josep Farré Lladós<sup>2,4</sup> · T. Staffan Lundström<sup>1</sup> · Erik Höglund<sup>2</sup>

Received: 30 December 2016 / Accepted: 8 May 2017 / Published online: 19 May 2017  
© The Author(s) 2017. This article is an open access publication

**Abstract** In this paper, numerical simulations of lubricating grease flow in the grease pocket of a double restriction seal geometry using computational fluid dynamics are presented. The grease is treated as a single-phase Herschel–Bulkley fluid with different rheological properties corresponding to NLGI grade 00, 1 and 2. The numerical code and rheology model have been validated with a semi-analytical solution based on flow measurements using microparticle image velocimetry. The flow has been modelled for low and high rotational speeds driving the flow, and elevated temperatures. Also, the evolution of contaminant particles in the grease pocket is investigated. It was found that the flow and velocity distribution in the pocket—and consequently the contaminant particle concentration evolution, is characterized by the shear thinning rheology of the grease. With higher shear rates in the grease and higher temperatures, the grease approaches a more Newtonian type of behaviour leading to a reduced yield and shear thinning characteristics directly affecting the grease ability to transport contaminant particles.

**Keywords** Lubricating grease flow · Velocity profiles · Rheology · Lubrication · Computational fluid dynamics (CFD) · Double restriction seal · Contaminants

## 1 Introduction

In many mechanical components like bearings, gears and seals, grease is used to lubricate the moving parts. Compared to oil, lubricating grease has many advantages as it due to its consistency adheres as well as coheres to the surfaces and thereby prevents corrosion and leaking. The quality of the lubrication is dependent on the grease motion in the actual application, and in order to design mechanical components such that an optimum lubrication is enabled an understanding of the grease flow dynamics is important. The flow in grease-lubricated mechanical systems like rolling element bearings is inherently very complex with a huge span of shear rates present, and the flow characteristics are also varying from wall-bounded flows important, e.g. for the flow in seals, to deformable, free-surface flows important for the re-lubrication process and inside bearings as they typically only are filled to about 30% to avoid heavy churning. Modelling grease flow analytically is only possible in simple geometries like channels, pipes and cylinders; see, for example, Westerberg et al. [1] and Li et al. [2, 3], for grease flow models in rectangular channels and concentric cylinder configuration, and Cheng et al. [4]; Sisko [5] for flow in a pipe. For more complex flows, numerical models are needed. Computational fluid dynamics (CFD) has shown to be a powerful tool in numerous applications and flow scenarios over the years and is a tool which has increased enormously in capacity with the increasing computational capacity. For grease flow however, studies where CFD is used is scarce in the

---

This article is part of the Topical Collection on STLE Tribology Frontiers Conference 2016.

✉ Lars G. Westerberg  
lars-goran.westerberg@ltu.se

<sup>1</sup> Division of Fluid and Experimental Mechanics, Luleå University of Technology, 971 87 Luleå, Sweden

<sup>2</sup> Division of Machine Elements, Luleå University of Technology, 971 87 Luleå, Sweden

<sup>3</sup> Department of Mechanical Engineering, Indian Institute of Technology Patna, Bihta, Bihar 801103, India

<sup>4</sup> ETSEIAT, Universitat Politècnica de Catalunya, 08222 Terrassa, Spain

literature. This is much due to the complexity of the material by means of its multi-phase composition and non-Newtonian, shear thinning rheology. Also, with shear rates varying between  $10^{-2}$  and  $10^6 \text{ s}^{-1}$  [6, 7] it is a huge challenge capturing the full problem from the grease semi-solid, visco-elastic yield characteristics [8] at very low shear rates, to the flow properties at very high shear rates—which mainly is governed by the rheology of the base oil [6]. Further, CFD models where a fibre structure in the flow (for grease comprised by the thickener matrix) is continuously deforming do not exist to the author's knowledge. The fibre breakdown is a physical complex process where the fibres are broken in the contact points at low shear rates, while at high shear rates the fibres themselves experience a breakdown in height or length [9]. Another property of greases that adds to the complexity in obtaining reliable models is that the grease is affected by shear degradation [10] during long time of shear exposure. This is coupled to the evolution of the stress in the flow—which in addition to having a nonlinear relation to the shear rate—also is dependent on time, i.e. it is thixotropic [11]. This yield that the grease experiences an isothermal decrease in viscosity during shearing, and an increase in viscosity due to resolidification once the shearing ends [12].

The grease composition does not only affect its bulk flow properties, but also the dynamics close to the boundaries by means of wall slip. Westerberg et al. [1] showed evidence of slip close to the boundaries in a straight channel. Exactly what causes slip is still an open question and subject for debate. Czarny [13, 14] found that slip does not occur in the immediate vicinity to the wall, but rather inside a layer very close to the wall which is formed by an interaction between the grease thickener and the wall material. Since the thickener often is polar, a concentration gradient of thickener close to the wall is formed. Slip then is argued to occur in the layer with the highest concentration of base oil. These results are also in line with results by Vinogradov et al. [15] who concluded that slip is not due to material sliding against the wall, but rather is caused by a change of material properties close to the wall. These material properties typically are the increases in concentration of fibres (thickener), as stated by Czarny [13, 14]. However, additional conditions such as changed fibre orientation due to thixotropy [11] may contribute to wall slip. Further, the surface roughness of the solid boundary is assumed to have an impact on the slip properties [16]. Westerberg et al. [1] though found that a roughness (Ra-value) of the order of microns not affects the slip effect. By means of numerical modelling, the slip can be included by implementing a slip length (i.e. thickness of the slip layer) and a slip velocity. Building a numerical model that includes the physical onset of slip

would require a full model of the grease/solid boundary interface on virtually molecular scale, also including a model for oil bleeding.

In terms of flow visualizations and numerical modelling of lubricant flow in bearings, little has been done on full geometries. Lubricant flow in journal bearing supply pocket using particle image velocimetry (PIV) technique had been performed by Kosasih et al. [17]. They demonstrated the use of PIV on difficult geometrical configuration and proposed a correction procedure when an endoscope is used. They also aimed to shed some knowledge about flow field in journal bearing supply pocket. But the flow field inside the journal bearing is missing. Being able to numerically model the full grease flow (i.e. a model covering the full range of shear rates) in a geometry such as a ball bearing would be very valuable in the design. A first approach to develop such models has been made by Sarkar et al. [18], where lubricating grease flow has been modelled in a straight channel with a rectangular cross section. In that study, the grease is modelled as a single-phase Herschel–Bulkley fluid with values of the rheological parameters obtained from rheometer tests of Lithium greases with NLGI grade 00, 1 and 2, respectively. The study comprises investigation of the flow in an unrestricted and restricted channel, respectively, where the numerical model has been validated towards analytical models and data from flow visualizations using micro-PIV ( $\mu\text{PIV}$ ). Also, the motion of contaminant particles placed in the flow was investigated. In this study, the numerical model is developed to cover the flow in a concentric cylinder configuration, resembling a double restriction seal (DRS). Here, the grease flow that was experimentally and analytically investigated/ modelled by Li et al. [3] and Baart et al. [19] is modelled numerically using COMSOL Multiphysics. The approach is analogous to the work in Sarkar et al. [18] as the velocity profiles are validated against  $\mu\text{PIV}$  measurements. The flow has then been modelled for higher speeds of the rotating shaft driving the flow. The evolution of how particles inserted into the flow migrate in the flow is also modelled together with the leakage flow on the velocity profiles. As for the particle transport analysed in Sarkar et al. [18], the purpose of this investigation is of particular interest with respect to how contaminant particles which enter the actual geometry travel through the seal.

## 2 Methods

### 2.1 Governing Equations, Rheology Model(s) and Greases

COMSOL Multiphysics v5.2 (hereafter just referred to as 'Comsol' for simplicity) [20] has been used for the

numerical modelling. In Comsol, the apparent viscosity is a function of the shear rate (denoted  $spf.sr$ ), which is implemented in the numerical code, enabling any rheology model to be implemented. In the present study, the grease

is described as a single-phase, isothermal continuous fluid, with the Navier–Stokes equation and the continuity equation governing the flow.

For a stationary flow, the governing equations reads (as implemented in Comsol)

$$\rho(\mathbf{u} \cdot \nabla)\mathbf{u} = \nabla[-p\mathbf{I} + \mu(\nabla\mathbf{u} + (\nabla \cdot \mathbf{u})^T)] + \mathbf{F} \quad (1)$$

$$\nabla \cdot \mathbf{u} = 0, \quad (2)$$

**Table 1** Rheological parameters for respective grease based on the Herschel–Bulkley rheological model [3].  $\tau_0$  is the yield stress,  $K$  the grease consistency,  $n$  the power law index ( $<1$  for greases),  $\rho_g$  the density of the greases

Grease	$\tau_0$ (Pa)	$K$ (Pa s)	$n$	$\rho_g$ (kg/m <sup>3</sup> )
NLGI 00	0	1.85	1	890
NLGI 1	189	4.1	0.797	910
NLGI 2	650	20.6	0.605	930

where  $\mathbf{u}$  is the velocity vector,  $\rho$  the density,  $\mu$  the dynamic viscosity (which is a function of the shear rate and where the shear rate/viscosity relation is governed by the actual rheology model),  $\mathbf{I}$  the identity tensor, and  $p$  the pressure.  $\mathbf{F}$  is a volume force, such as gravity (neglected here), centrifugal or electromagnetic forces. Continuity yields that

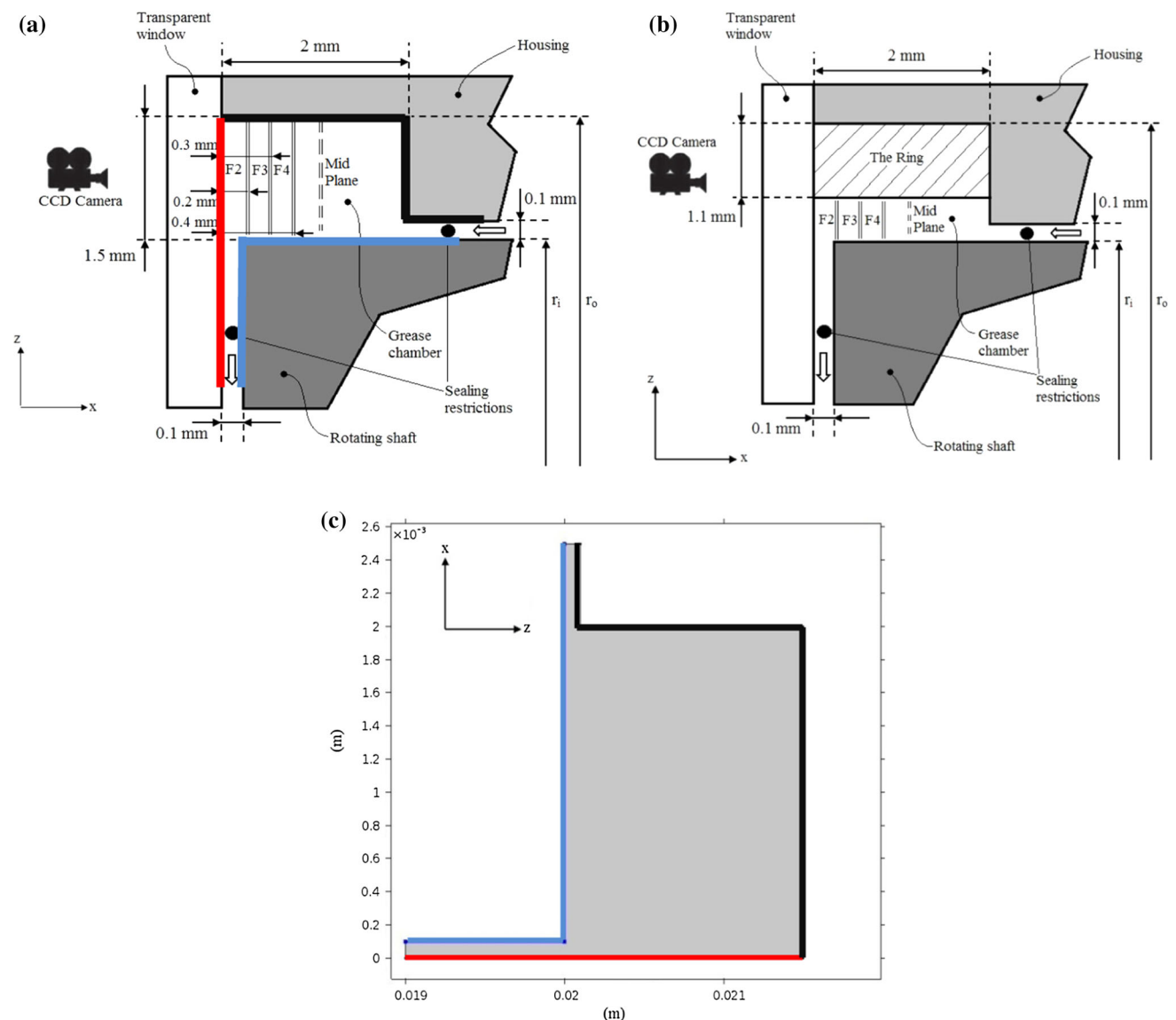


**Fig. 1** Double restriction seal (DRS) geometry and its grease pocket. **a** DRS without ring, **b** DRS with ring narrowing the pocket width, and **c** the grease pocket as modelled in Comsol. *Blue* boundary: rotating shaft, *red*: glass window, *black*: stationary housing (Color figure online)

the divergence term in Eq. (1) vanishes reducing the N–S equation to

$$\rho \mathbf{u} \cdot \nabla \mathbf{u} = -\nabla p + \nabla \cdot \mu(\nabla \mathbf{u}). \tag{3}$$

The modified Herschel–Bulkley rheology model [21] is considered. It reads

$$\mu = \frac{\tau_0}{\dot{\gamma}} (1 - e^{-m\dot{\gamma}}) + K\dot{\gamma}^{n-1}. \tag{4}$$

Here  $\tau_0$  is the yield stress,  $\dot{\gamma}$  the shear rate,  $K$  the grease consistency,  $n$  the shear thinning (or thickening) index, and  $m$  a model constant. The term in brackets including the exponential (transition) function with the model constant

enables to numerically capture a smooth transition from stationary, non-yielded grease, to moving yielded grease. This is needed as the H–B model includes the yield stress as a discrete threshold value, which indeed is a good engineering model but which physically is crude [6], and numerically, it causes problem as the transition from non-yielded to yielded grease switch at a given shear stress value. Comsol has the Carreau- and Cross rheology models implemented, which both generally are better alternatives in the limit of very low-, or very high shear rates as the zero- and infinite shear rate grease viscosity are included in the models. The Carreau model is defined as:

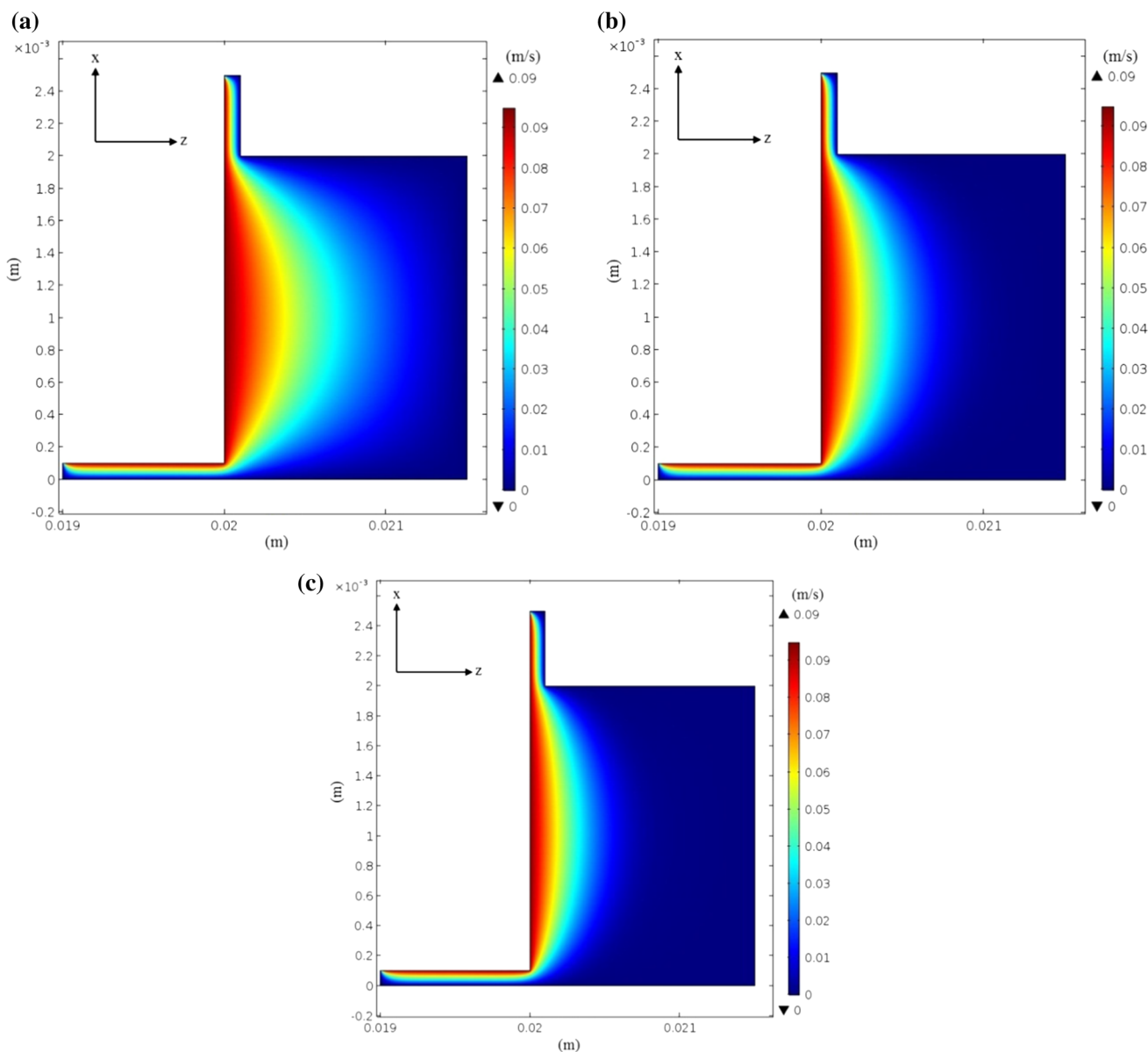


Fig. 2 Surface plot velocity of the three greases at the DRS grease pocket without ring. Shaft speed 0.095 m/s

$$\eta = \eta_\infty + \frac{\eta_0 - \eta_\infty}{\left[1 + (K\dot{\gamma})^2\right]^{\frac{n-1}{2}}}, \tag{5}$$

where  $\eta_\infty$  is the viscosity plateau at high shear rates,  $\eta_0$  the viscosity plateau at low shear rates,  $\dot{\gamma}$  the shear rate,  $K$  the grease consistency and  $n$  the power law exponent. Considering  $\eta_\infty$  as zero Eq. (5) reads

$$\eta_d = \frac{\eta_0}{1 + (K\dot{\gamma})^{1-n}}, \tag{6}$$

which equals the Cross rheology model. The Herschel–Bulkley rheology model works well between the low and high shear rate plateaus in a viscosity/shear rate plot [6] and also works well in analytical modelling as it has a

fairly simple relation between the viscosity and the shear rate. For the shear rates present in present flow cases, the H–B model is valid; it was also found by Sarkar et al. [18] that the H–B model best captures the plug flow behaviour of the grease. The greases used in the experiments are all fully formulated commercial greases with rheology presented in Table 1.

In this study, a physics-controlled mesh with extra fine element size has been used to discretize the fluid domain. The total number of elements is 18,718 considering 17,374 triangular elements and 1344 quadrilateral elements. There are 676 edge elements and 8 vertex elements. A steady 2D axisymmetric, single-phase laminar flow module is used with a PARIDOS scheme to solve the systems of equations.

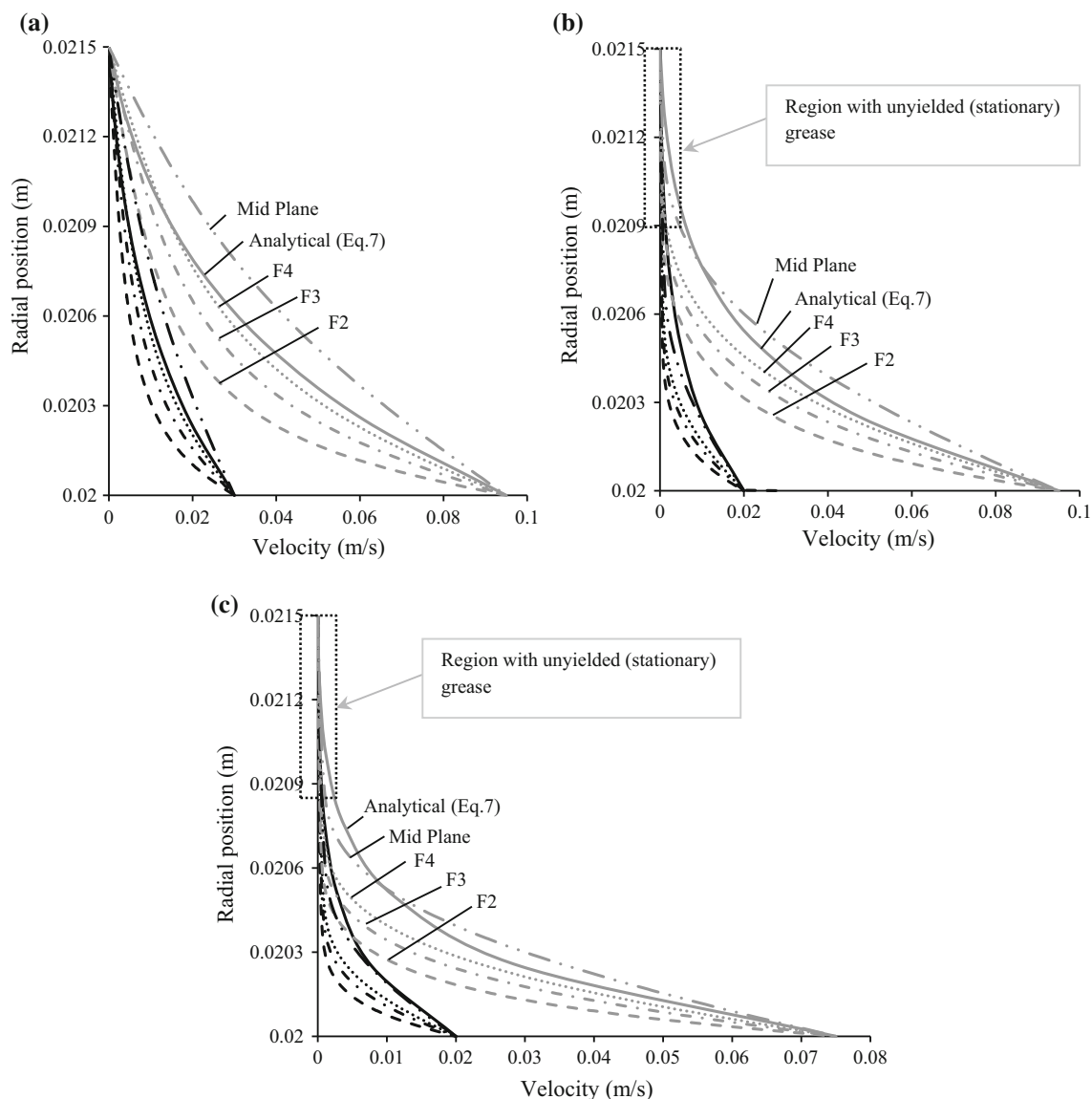


**Fig. 3** Velocity profiles in the grease pocket for low shaft speed (*black*) and high shaft speed (*grey*). F2–F4 represents the focal planes in Fig. 1. The mid-plane is the plane at the centre of the grease pocket. The *curve line* style is the same for both low and high shaft speeds

A rotating wall boundary condition is applied at the shaft surface (blue boundary in Fig. 1) corresponding to the velocity of the rotating shaft  $r_i\omega_i$ , where  $r_i$  is the radius of the rotating shaft ( $=20$  mm), and  $\omega$  is the angular velocity which in the present study is in the range of 1–3.75 rad/s. Here, no slip is assumed as a boundary condition at the wall representing the stationary housing (black boundary), and the glass window (red boundary). For the case of leakage flow, denoted by the arrows in the sealing restrictions in Fig. 1, an inflow rate is set, while for no leakage flow no slip is assigned at the inflow and outflow boundaries. The convergence criterion for the solver is set to  $10^{-6}$ , i.e. a relative error of 0.0001%, which for the

simulations in this paper has been obtained after maximum 25 iterations.

### 2.2 The Double Restriction Seal (DRS) Geometry

In the DRS, a grease pocket is formed between a rotating shaft and a stationary housing. Figure 1 shows the two versions of the DRS considered in this paper; one without ring where the full pocket volume is used, and one with a ring which shortens the distance between the rotating shaft and stationary housing enabling a 1D flow in the pocket. In this paper, we investigate both the cases with a negligible transverse (leakage) flow, and the impact of the leakage

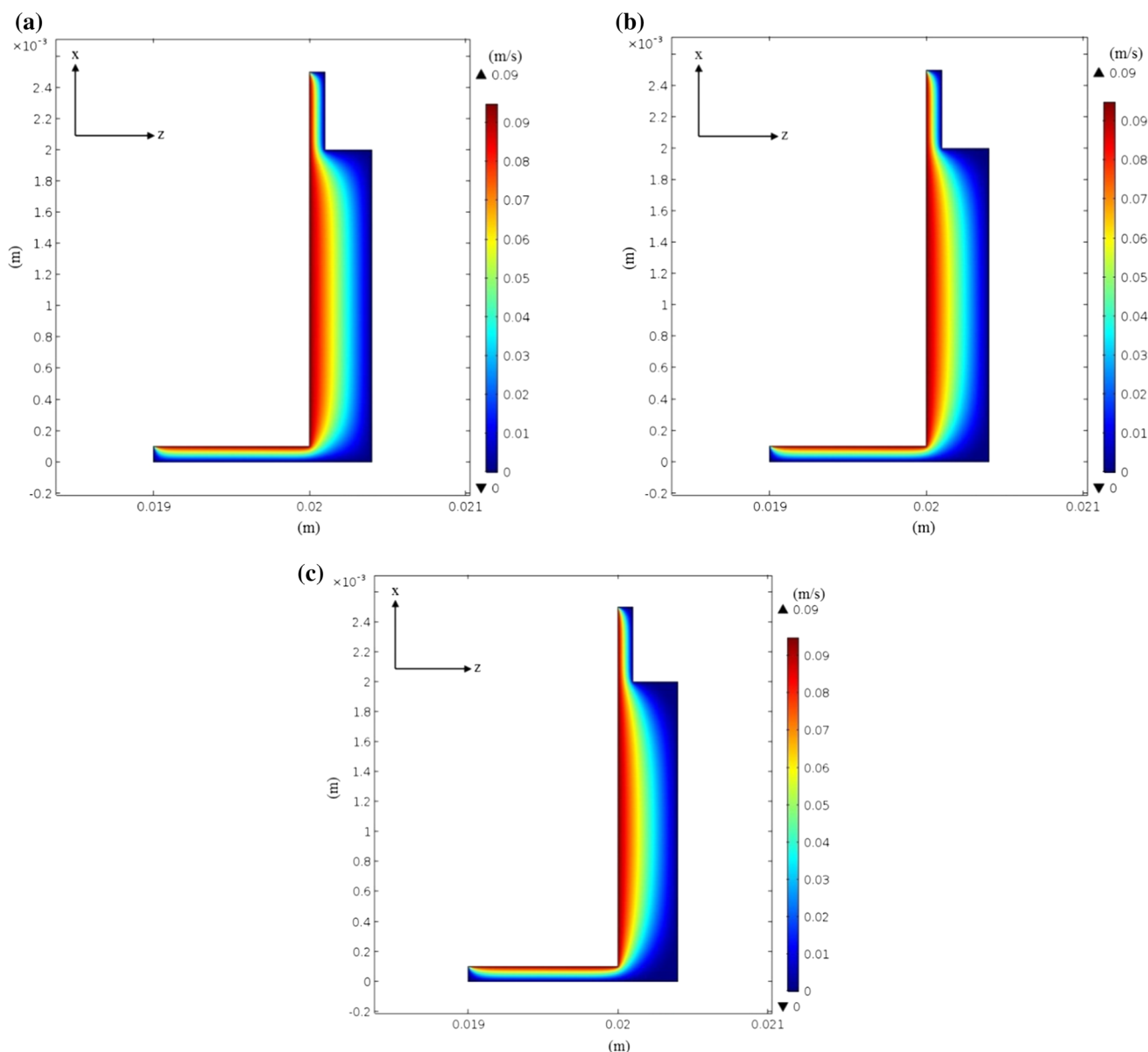
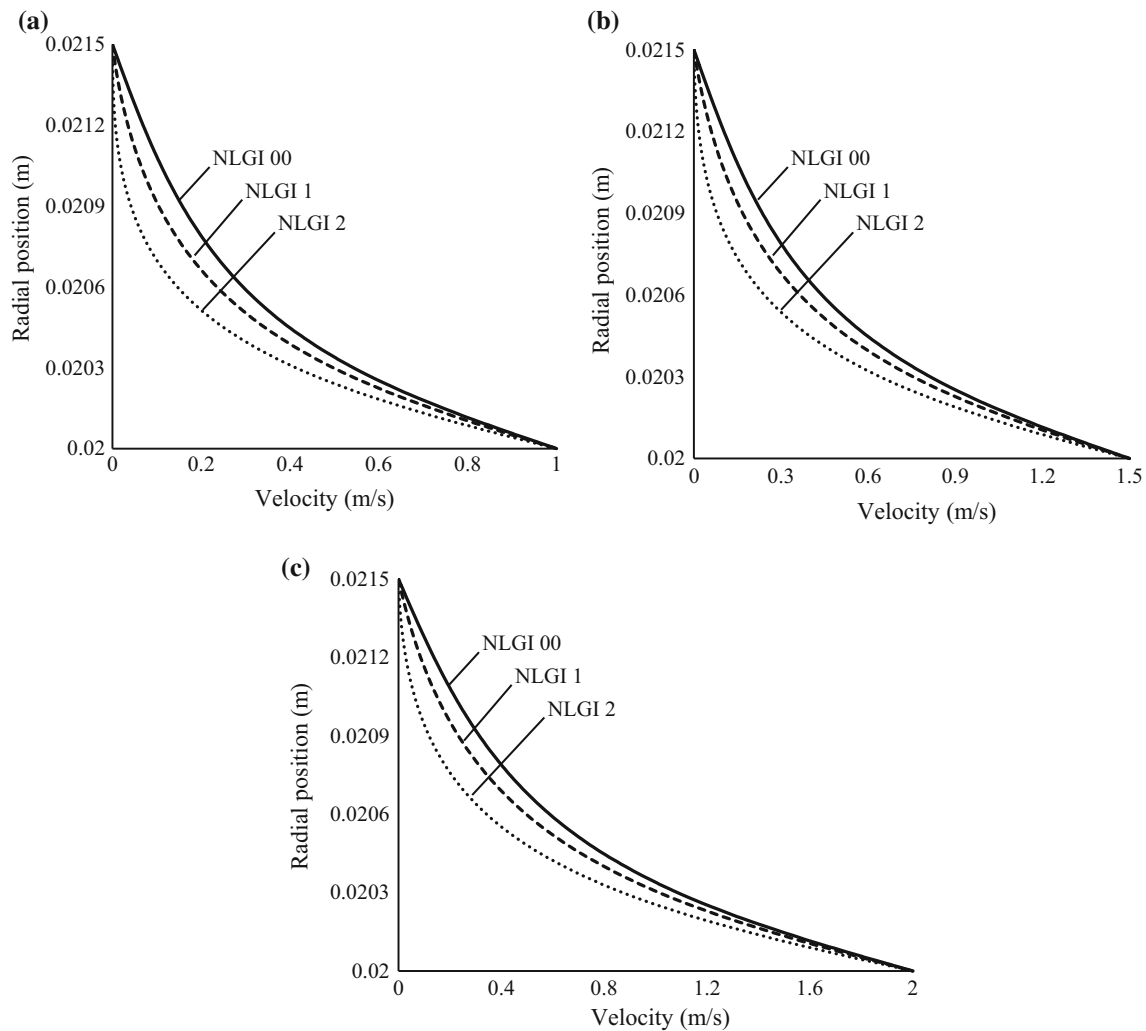


Fig. 4 Velocity surface plot in the grease pocket with ring. Shaft speed 0.095 m/s



**Fig. 5** Velocity profiles in the grease pocket at higher shaft speeds

flow on the velocity profiles in the grease pocket. For respective grease, the shaft speed varies according to: 0.030–0.095 m/s (NLGI 00), 0.020–0.095 m/s (NLGI 1) and 0.020–0.075 m/s (NLGI 2).

The geometry without ring is the same as in Baart et al. [19] where flow measurements using  $\mu$ PIV in the grease pocket without ring are presented together with a semi-analytical model of the flow. For the grease pocket without ring, the width is almost equal to the height. This means that the side walls have a significant influence on the grease velocity profile as shown by Baart et al. [19], i.e. the flow is dependent on both the  $r$  and  $x$  coordinates (2D flow). In the present study, the full dimensions of the grease pocket are numerically modelled and validated by comparing the velocity profiles with the model developed by Baart et al. [19], who in turn have validated the model against experimental data from  $\mu$ PIV measurements. The present numerical model is validated by comparing the velocity profiles at the different planes defined in Fig. 1.

In the work by Baart et al. [19], the measurements are described to be taken at a distance of 0.2 mm from the transparent window wall. This distance is, however, subject to uncertainty as the limited transparency of the grease makes it difficult to determine the exact location of the plane of measurement.

### 3 Results and Discussion

#### 3.1 Validation of Numerical Grease Flow Model with Results by Baart et al. [9]

In order to investigate the impact of the end walls along the  $x$ -axis in Fig. 1, the exponential velocity flow from Baart et al. [19] is considered. Baart et al. [19] developed a semi-analytical model for the grease flow in the grease pocket without ring where the expression for the velocity as function of the  $r$ -coordinate reads

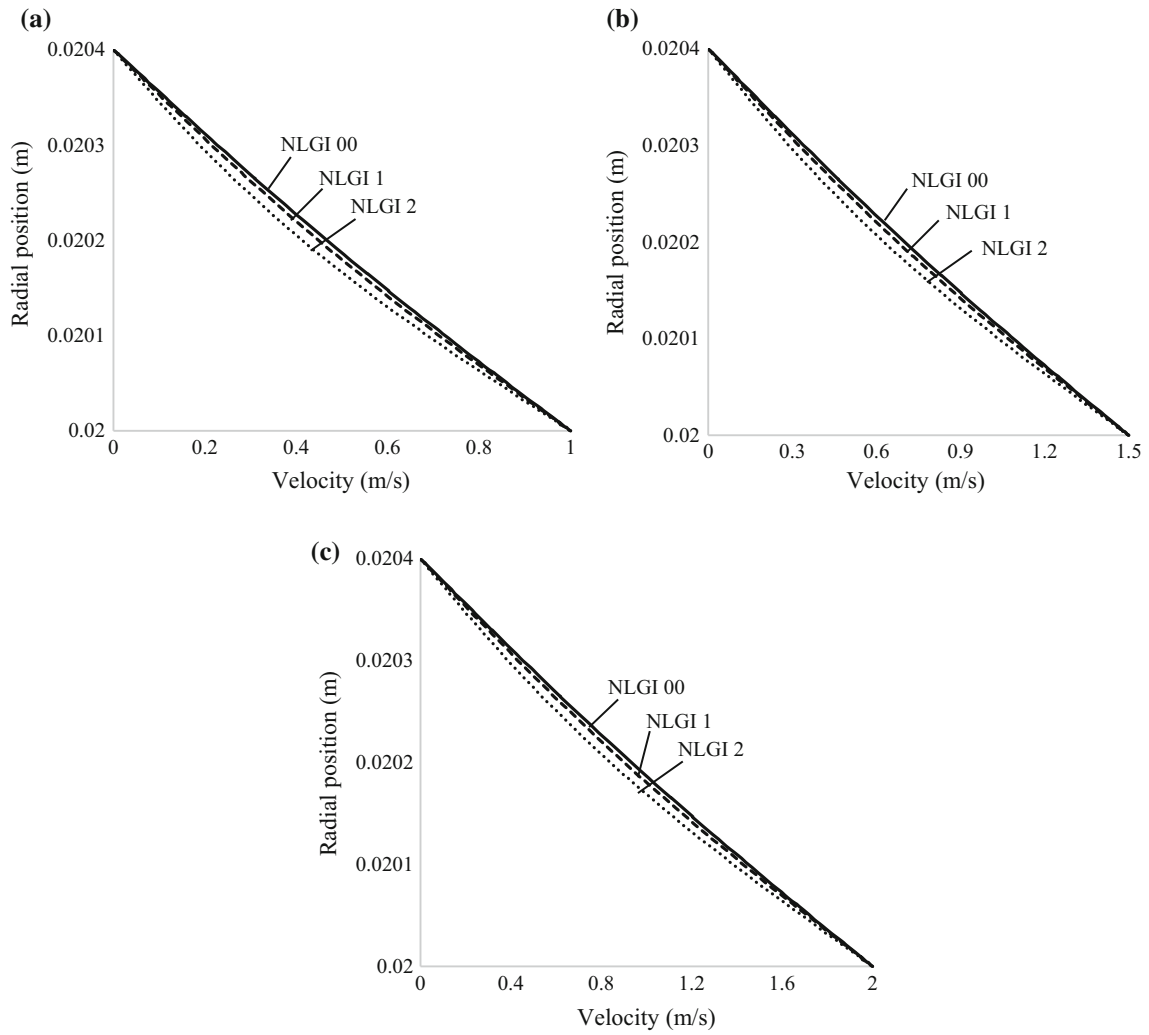


**Fig. 6** Velocity profiles in grease pocket with ring at higher shaft speeds

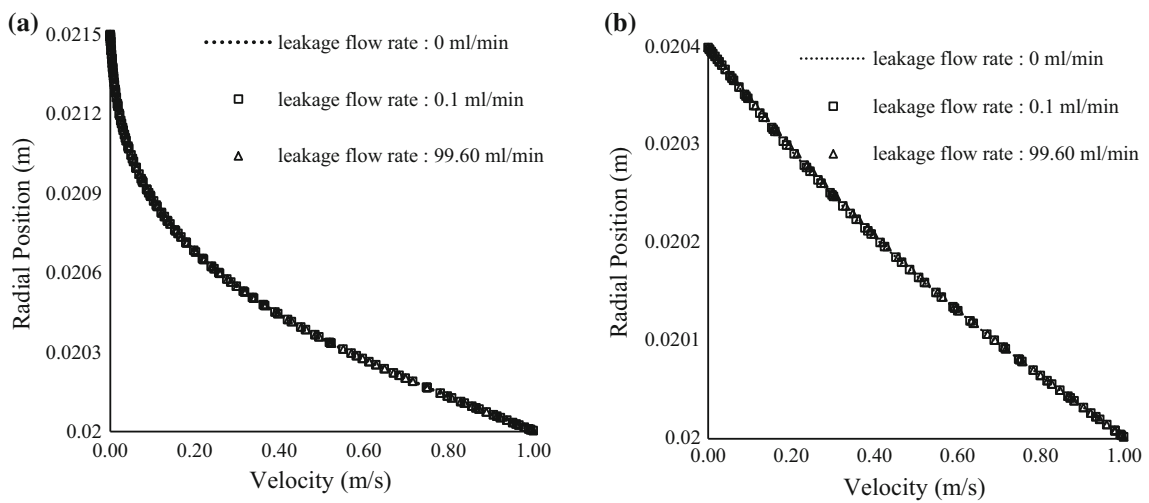


**Fig. 7** Velocity profiles at shaft speed 1 m/s **a** for axial DRS, **b** for axial DRS with ring using NLGI 2 grease. *Dotted* with zero leakage flow rate, *open square* 0.1 ml/min, *open triangle* 99.60 ml/min leakage flow rate



**Table 2** Rheological parameters for NLGI 2 grease at different temperatures based on the Herschel–Bulkley rheological model [22]

Temperature (°C)	$\tau_0$ (Pa)	$K$ (Pa s)	$n$ (-)
25	500	26	0.43
50	280	14.5	0.56
70	180	8	0.70

In Ref. [22], there is an error in the corresponding table showing the rheology data. The values for the consistency index  $K$  and  $n$  are in wrong order with respect to increasing temperature

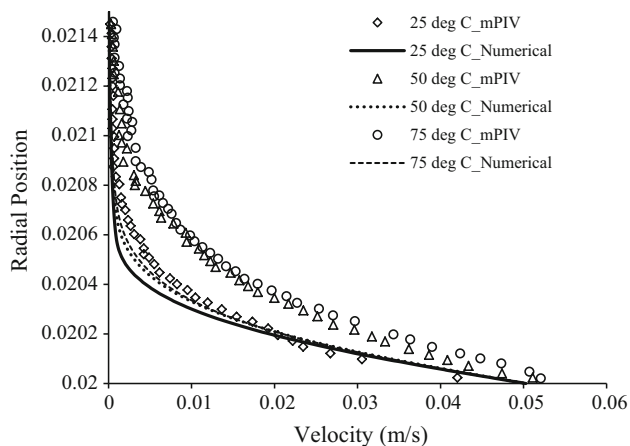


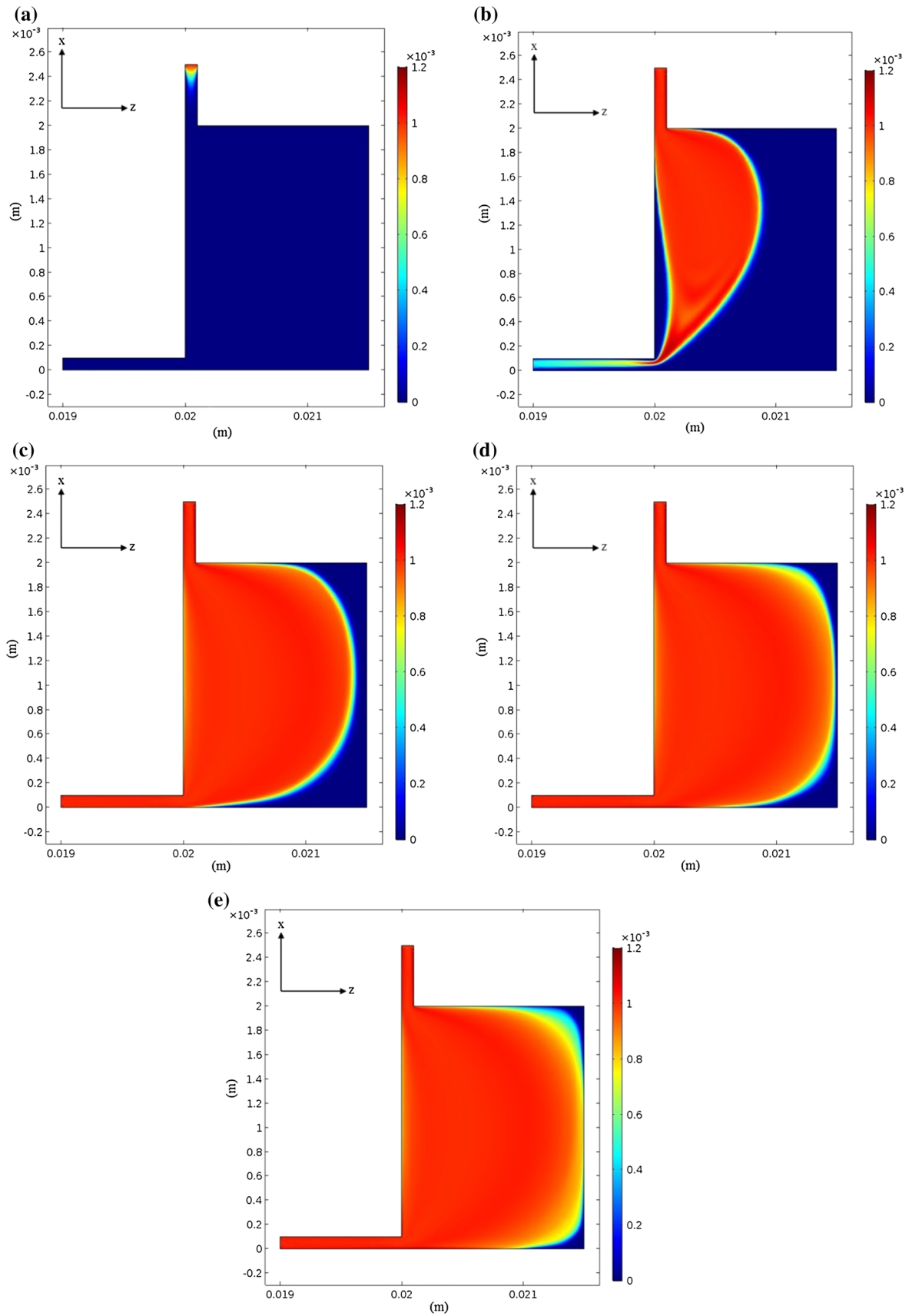
**Fig. 8** Comparison of measured and numerical velocity profiles for NLGI 2 grease at different temperatures; *open diamond* 25 °C, *open triangle* 50 °C, *open circle* 75 °C using numerical and *solid* 25 °C, *dotted* 50 °C, *dashed* 75 °C using mPIV. The PIV data are from Ref. [19]

$$u(r) = U_s e^{\alpha(r-r_i)} \left[ \frac{r_o/r - r/r_o}{r_o/r_i - r_i/r_o} \right]. \tag{7}$$

This expression is a function of the solution for the Newtonian flow in identical geometry ( $=U_s[\dots]$ ), and the exponential function imposing the identified exponential form of the velocity profile by Baart et al. [19]. The exponential behaviour is resulting from the shear thinning rheology of the grease. In Eq. (7),  $U_s$  is the rotating shaft speed,  $r_o$  the outer radius ( $=0.0215$  m),  $r_i$  the inner radius ( $=0.02$  m) and  $\alpha$  a constant (fitting parameter) for each grease with the unit  $m^{-1}$ . The alpha value was found to be  $-3000$ ,  $-2000$  and  $-1000$  for the NLGI 2, 1 and 00 greases, respectively. Important to emphasize is that Eq. (7) is not valid throughout the whole grease pocket with a unique alpha value; it is valid at the same location (plane) as the  $\mu$ PIV measurements have been performed. This as the alpha value emerges from the fit with a  $\mu$ PIV velocity profile, which is obtained at a unique plane (cf. the planes in Fig. 1).

The velocity surface plot for the flow in the grease pocket without ring is shown in Fig. 2. The driving shaft

speed is 0.095 m/s for all three greases. The trend for the evolution of the grease flow towards the housing wall with increasing grease consistency is clear, with a significantly larger part of the grease pocket being yielded for the soft NLGI 00 grease compared to for the NLGI 2 grease. This result is in line with the results by Baart et al. [19] and Li et al. [3] who showed that the grease velocity profiles experience a significant nonlinearity due to the shear thinning effects. In order to investigate this further and to validate the numerical results, the velocity profiles at respective plane (Fig. 1) are plotted and compared to the semi-analytical model in Eq. (7); see Fig. 3. As Baart et al. [19] have matched this model to experimental data for the actual shaft speeds, the velocity profiles from the  $\mu$ PIV measurements are not shown; the case of elevated temperatures (Fig. 8) is excepted. Figure 3 shows a comparison between the analytical and numerical velocity profiles at the different planes (F2–F4 and mid-plane; cf. Fig. 1) for the three greases. The solid line represents the analytical model (Eq. 7), while the dashed lines represent the velocity profiles from the numerical model at respective plane. Two shaft speeds have been considered: the velocity profiles for the lower shaft speed is in black, while the velocity profiles for the higher shaft speeds are in grey. As shown in Fig. 3, there is a difference between the analytical and numerical velocity profiles at the F2 plane, recalling that the  $\mu$ PIV measurements are stated to be at the plane 0.2 mm ( $=F2$ ) from the glass wall. From the simulations, it is more likely that the plane is located at a distance greater than 0.2 mm from the glass wall, closer to plane F4 which is 0.3 mm from the glass wall. The trend is that the deviation between the semi-analytical model and the results from the simulations increases with increasing NLGI grade: for the NLGI 00 grease the numerical model for plane F4 matches the semi-analytical model well, while for the NLGI 2 grease plane F4 matches the semi-analytical model closer to the rotating shaft (i.e. high shear rates), and the mid-plane closer to the stationary housing (low shear rates). This result is most likely due to the shear thinning property of the grease and not the least due to the occurrence of shear banding in the flow. Wall slip may also have an (minor) impact on the flow. Physically, these two phenomena are related to the composition of the grease. As addressed in Introduction, wall slip has been explained both by means of a thin layer of base oil having been bled out in the grease/solid boundary contact, and an increased thickener gradient close to the boundary. Shear banding is a result of discontinuous shear in the flow due to locally varying rheological properties, which in turn is a result of local fibre deformation/orientation and oil concentration. Modelling this numerically requires a multi-phase model of the grease, including how the thickener matrix deforms under the applied shear, and a model for how the oil flows (bleed)



◀ **Fig. 9** Contaminant volume fractions for axial DRS using NLGI 2 grease at different times. Here  $U_s = 1$  m/s

through the thickener fibre network. Both the fibre deformation and oil flow are really challenging scientific tasks and part of the vision of having complete models of the grease flow for the full range of shear rates present in a bearing. So in this context shear banding and wall slip are not actual in the present paper. However, the effect of wall slip on the velocity profiles can be modelled by applying a specified slip velocity and slip length. In order to obtain best possible fit between the velocity profile from the numerical model and the experiments, the slip length and slip velocity can of course be elaborated with, but as shown in Westerberg et al. [1]; Li et al. [3] the slip length and slip velocity are so small that it can be considered negligible in context with the bulk flow. Another error source as originally addressed in Westerberg et al. [1] is that the rheological parameters in Table 1 are incorrect due to the very same effects discussed here (wall slip and shear banding). The rheometer assumes ideal conditions where no such non-ideal effects are present; any presence of wall slip or shear banding will result in erroneous results. Further, for the NLGI 1 and 2 greases (especially for lower shaft speed) there is a region of unyielded (stationary) grease in connection to the stationary housing. An error source causing the deviation between the numerical model and experiments/analytical model may argue to be is how the transition from stationary to moving (flowing) grease is modelled: apparent is that the transition is gradual (continuous), which is not captured by the H–B model in its original form. The deviation is, however, most dominant in the bulk flow, meaning any flaws in the transition function should not impact the solution. The dynamics in the transition from unyielded to yielded grease may though still contribute to the observed difference as, e.g. base oil or thickener gradients in connection to the transition may play a role.

In Fig. 4, the velocity surface plot for the flow in the grease pocket with ring is shown. Compared to the flow in the pocket without ring (Fig. 3), there are two major differences by means of a larger percentage of the pocket having yielded (moving) grease, and a large part of the pocket having a flow which is independent of the vertical coordinate, i.e. the flow is one-dimensional as the impact of the top and bottom boundaries vanishes at some distance away from these. A greater part of the pocket being yielded is due to the distribution of shear forces in the pocket. With a reduced gap, the shear in the flow transferred from the rotating shaft is greater compared to the pocket without ring.

### 3.2 Flow for Higher Shaft Speeds, Elevated Grease Temperature, and Increased Leakage Flow Rate

A drawback with the DRS test rig is that it has limitations in terms of shaft speed; the maximum speeds are the ones considered in previous section. With a working numerical model, it is hence of interest to investigate the flow for increased rotational speeds, the impact of an elevated temperature on the flow, and how an increased leakage flow affect the velocity profile. Here higher speeds of 1, 1.5 and 2 m/s have been considered, and the velocity profiles are plotted in Figs. 5 and 6 for the case without ring and with ring, respectively. It is evident that the increase in shear rate due to the increased shaft speed for respective case with or without rings has no significant influence on the velocity profiles even though the NLGI 2 and 1 profile tend to move towards the NLGI 00 velocity profile. However, for the case with ring the thickest grease shows a velocity profile very similar to the Newtonian-like NLGI 00 grease. These results match the results in Westerberg et al. [1] where it for the flow in a straight channel is shown that the velocity profile for the NLGI 2 grease approaches the Newtonian-like velocity profile of the NLGI 00 grease when the shear rate in the flow increases.

To observe the effect of higher leakage flow, the outlet flow at the bottom boundary is considered as 0 ml/min, 0.1 ml/min ( $=1.66 \times 10^{-9}$  m<sup>3</sup>/s) and 99.60 ml/min ( $=1.66 \times 10^{-6}$  m<sup>3</sup>/s). Figure 6 shows the velocity profile at different outlet flows. It is clear that the higher leakage flow does not affect the velocity profile (Fig. 7).

For flow at elevated temperatures, the grease rheology changes. The numerical model is based on the grease rheology at the actual temperatures rather than performing a heat transfer model. In this part the effect of temperature on the NLGI 2 grease rheology is presented. The rheology of the grease, based on the H–B rheology model, is presented in Table 2.

Figure 8 shows a comparison between the numerical and measured velocity profiles at 25, 50 and 70 °, respectively. With the increase in temperature the yield stress of the grease decreases and the grease becomes less shear thinning; i.e.  $n$  increases. In other words, the grease rheology approaches a more Newtonian character as the temperature increases. This is also mirrored in the development of the velocity profiles with increasing temperatures, where the parabolic shape is decreasing. Also, in general the match between the numerical model and PIV data is better for higher temperatures. This is in line with the discussion in Sect. 3.1 as the increased yield characteristics at lower temperatures are likely to complicate the deformation of the grease in a way which is not described fully by the rheology model; therefore, there is an increase in grease flow velocity profile.

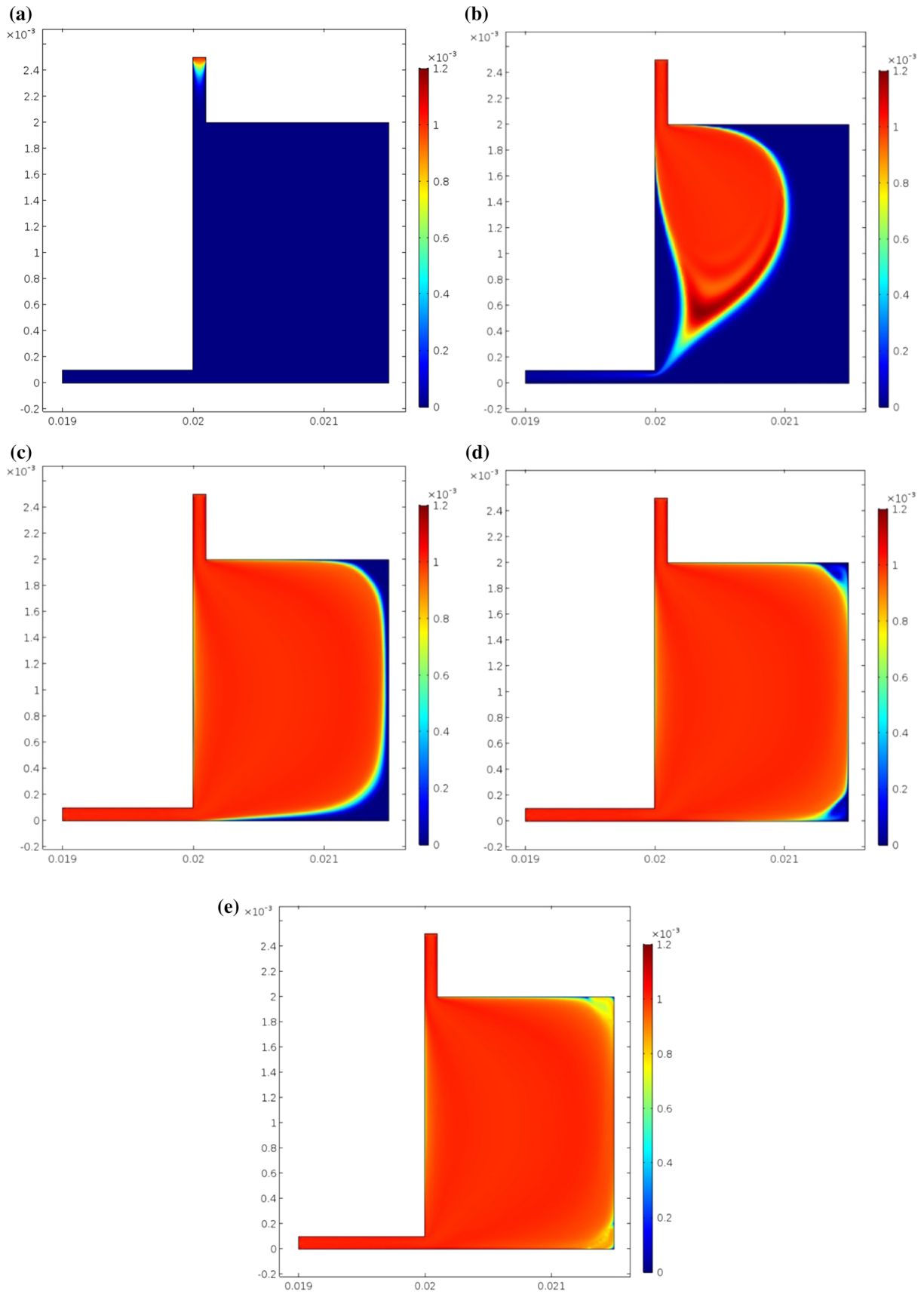


**Fig. 10** Contaminant volume fractions for axial DRS using NLGI 00 grease at different times when  $U_s = 1$  m/s

### 3.3 Contaminant Migration

Considering the sealing function in a double restriction seal geometry, Baart et al. [19] suggest that solid contaminant particles present in the flow first pass through the top sealing restriction (Fig. 1c) and then get stuck in the grease pocket and therefore reduce the probability of particles passing through the second restriction. Baart et al. [19]

derived a mathematical model for contaminant migration and illustrated that the solid contaminant particles having a larger density than the grease consequently migrate to large radius in the pocket due to centrifugal forces. In order to investigate contaminant migration through the double restriction seal geometry, a multi-phase flow has been analysed using a mixture-model laminar flow in this paper. This is done by applying a slip model as homogeneous flow and activating the swirl flow option in Comsol v5.2. Density ( $\rho_{cp}$ ), radius ( $a$ ) and volume fraction of the dispersed phase, i.e. the solid contaminant particles, are

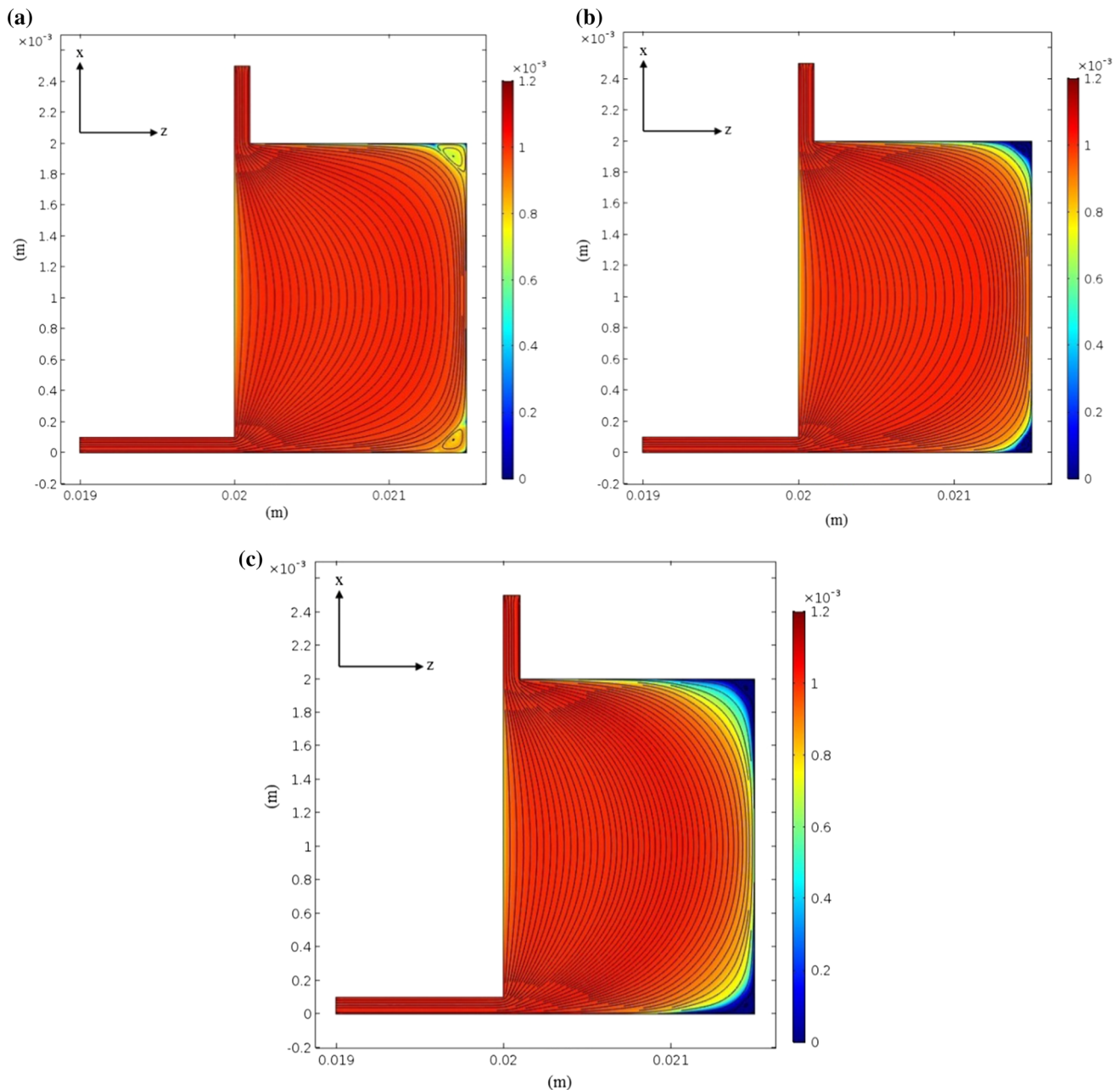


**Fig. 11** Mixture-velocity streamlines and solid-phase volume fraction at 100 h for axial DRS using three greases **a** NLGI 00, **b** NLGI 1 and **c** NLGI 2 when  $U_s = 1$  m/s

2100 kg/m<sup>3</sup>, 7 μm and 0.001, respectively [19]. Gravity has been applied in the grease domain. The volume force in the angular direction applied in the grease chamber as a function of the centrifugal forces per unit volume of the grease chamber, reads:

$$F_{\text{vol}} = \frac{4a^3 U_s^2 (\rho_{\text{cp}} - \rho_{\text{g}})}{3rw(r_o^2 - r_i^2)}. \quad (8)$$

Here  $w$  is width of the grease pocket, i.e. 2 mm. The mixture of grease and contaminant particles has been applied with a constant flow rate of 0.1 ml/min as the arrows indicate in Fig. 1a.

Figure 9 shows the contaminant concentration in the axial DRS geometry for the NLGI 2 grease at  $t = 0$  s,  $t = 100$  s,  $t = 1$  h,  $t = 10$  h and  $t = 100$  h, respectively. The contaminant enters through the top seal restriction at  $t = 0$  s and then approaches towards the grease chamber. The migration of the contaminants towards the outer wall is apparent as time elapses. As a result of the shear-induced migration and gravity, the solid-phase volume fraction approaches the value for maximum packing close to the right outer wall. In Fig. 10, the corresponding evolution for the NLGI00 grease is shown. The NLGI00 grease has a Newtonian type of rheology with zero yield stress and no shear thinning property, i.e. much unlike the NLGI2

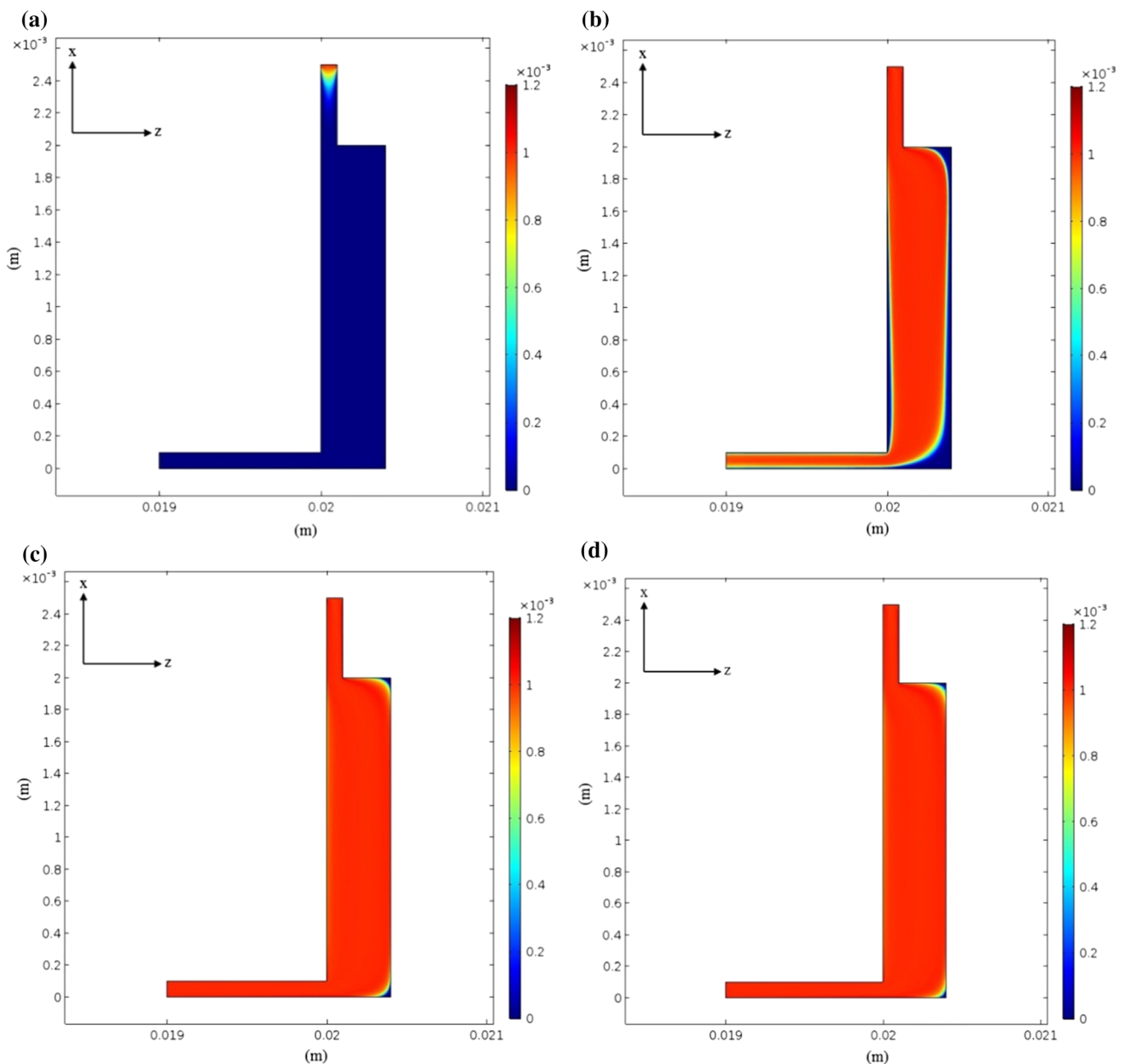


**Fig. 12** Contaminant volume fractions for axial DRS with ring using NLGI 2 grease at different running times when  $U_s = 1$  m/s

grease. A major difference between the particle migrations in the two greases is that for the NLGI00 grease a negligible volume fraction of the contaminants have reached the bottom seal restriction after 100 s, while for the NLGI2 grease the corresponding volume fraction is much higher. Another difference is that the whole grease pocket is filled with contaminants after 100 h in the NLGI00 grease. This also follows from Fig. 11 which shows that small recirculation areas are present in the corners for the NLGI00 grease, while the NLGI2 grease is stationary in these locations. The contaminant migration for three greases is

shown in Fig. 11. It indicates that the particle migrates fastest in the lowest consistency grease. In the high-consistency NLGI2 grease, which has the highest viscosity at low shear rates, the particle velocity has its minimum.

In Fig. 12, the contaminant concentration in the axial DRS with ring for the NLGI 2 grease at  $t = 0$  s,  $t = 100$  s,  $t = 1$  h,  $t = 10$  h and  $t = 100$  h is presented. It shows that particles migrate fast ( $t = 1$  h) in the grease pocket with ring compared to the grease pocket without ring. For the pocket with ring, the radial particle migration is almost equal (Fig. 13) and independent on the grease consistency.

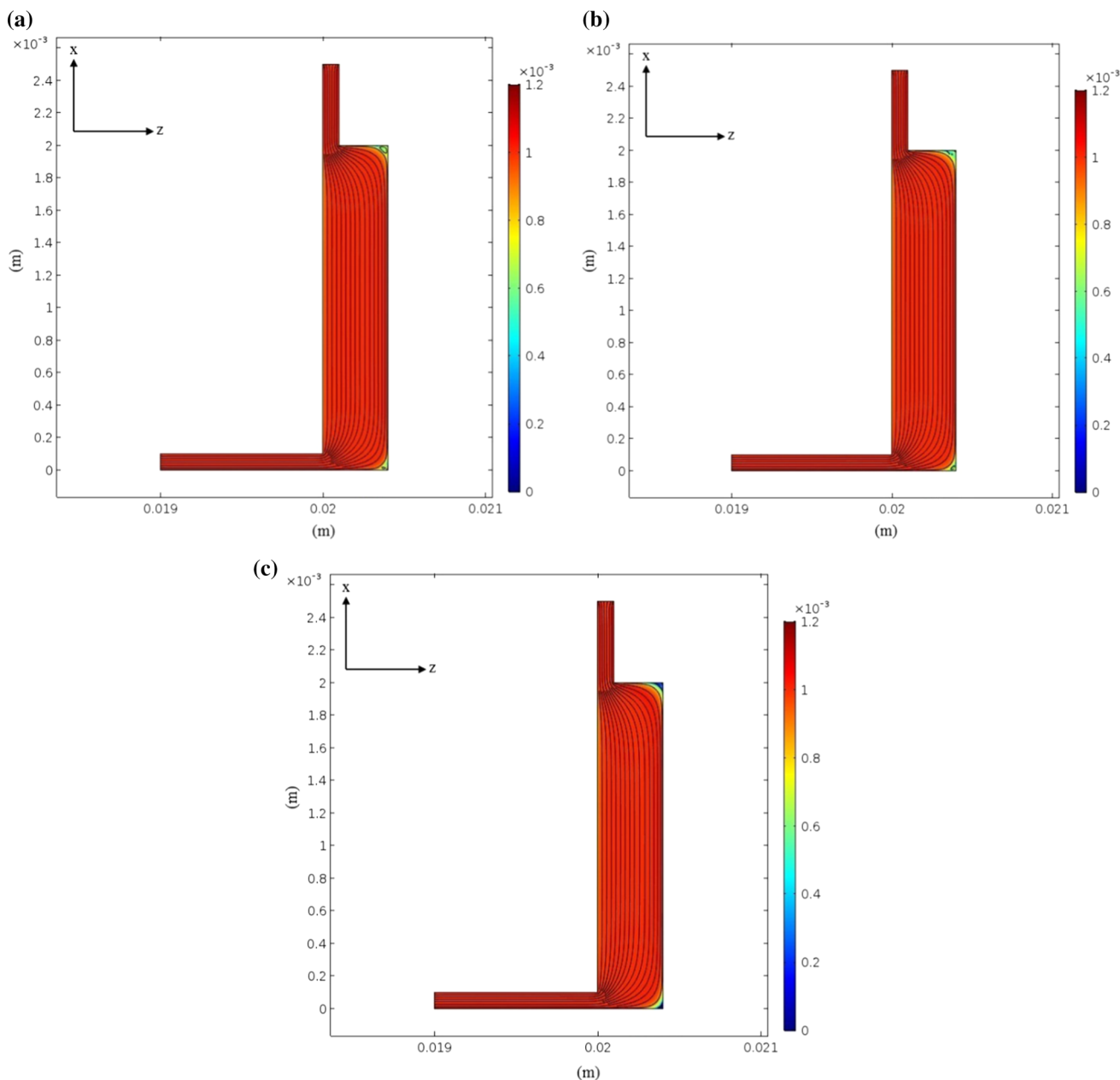


**Fig. 13** Mixture-velocity streamlines and solid-phase volume fraction at 100 h.  $U_s = 1$  m/s

This result matches well with the result on the velocity distribution in the pocket (Fig. 4), i.e. due to a higher shear in the flow the particles will fill the volume much faster.

#### 4 Concluding Remarks

This paper presents numerical modelling using computational fluid dynamics to analyse the flow motion of lubricating greases in a double restriction seal. The CFD model has been compared with a semi-analytical model based on experimental data from measurements using microparticle image velocimetry. Best agreement was found to exist for the case of a rheology where the yield stress and shear thinning are less pronounced, i.e. for less stiff greases and at elevated temperatures. The flow simulations enable modelling of the flow in more complicated geometries where analytical models cannot be obtained, neither flow measurements.

The following conclusions have been made from this research work.

- (a) The flow and velocity distribution in the pocket—and consequently the contaminant particle concentration evolution, is characterized by the shear thinning rheology of the grease. With higher shear rates in the grease and higher temperatures, the grease approaches a more Newtonian type of behaviour leading to a reduced yield and shear thinning characteristics directly affecting the grease ability to transport contaminant particles.
- (b) The fit between the semi-analytical and numerical models is better at elevated temperatures when the rheology approaches a more Newtonian-like characteristic with reduced shear thinning effect and reduced yield stress.
- (c) Wall slip is not likely to contribute to the observed difference in velocity profiles between the numerical model and experiments/semi-analytical model. Shear banding is more likely to contribute to the observed difference. This correlates with the observation that the match is better when the consistency of the grease is softer due to elevated temperature or less thickener content.
- (d) The migration of the contaminant particles towards the outer periphery in the grease pocket is apparent for all greases as time progresses. The particle migrates fastest in the lowest consistency grease which has the lowest viscosity at high shear rates.

**Acknowledgements** This project was funded by the Smart Machines and Materials program (SM<sup>2</sup>) at Luleå University of Technology. SM<sup>2</sup> is one of the University's strong innovation and research areas.

**Open Access** This article is distributed under the terms of the Creative Commons Attribution 4.0 International License (<http://creativecommons.org/licenses/by/4.0/>), which permits unrestricted use, distribution, and reproduction in any medium, provided you give appropriate credit to the original author(s) and the source, provide a link to the Creative Commons license, and indicate if changes were made.

#### References

1. Westerberg, L.G., Lundström, T.S., Höglund, E., Lugt, P.M.: Investigation of grease flow in a rectangular duct including wall slip effects using  $\mu$ PIV. *Tribol. Trans.* **53**, 600–609 (2010)
2. Li, J.X., Höglund, E., Westerberg, L.G., Green, T.M., Lundström, T.S., Lugt, P.M., Baart, P.:  $\mu$ PIV measurement of grease velocity profiles in channels with two different types of flow restrictions. *Tribol. Int.* **54**, 94–99 (2012)
3. Li, J.X., Westerberg, L.G., Höglund, E., Lugt, P.M., Baart, P.: Lubricating grease shear flow and boundary layers in a concentric cylinder configuration. *Tribol. Trans.* **57**, 1106–1115 (2014)
4. Cheng, Y., Pan, J., Yang, J.: Effect of thermorheological properties on shear flow of grease in pipes. *J. Chem. Eng. Jpn.* **49**, 815–823 (2016)
5. Sisko, A.W.: The flow of lubricating greases. *Ind. Eng. Chem.* **50**, 1789–1792 (1958)
6. Lugt, P.M.: Grease lubrication in rolling bearings, chapter 2. Wiley, Chichester (2013)
7. Cyriac, F., Lugt, P.M., Bosman, R.: Yield stress and low-temperature start-up torque of lubricating greases. *Tribol. Lett.* **63**, 1–10 (2016)
8. Barnes, H.A.: The yield stress: a review or ‘ $\pi\alpha\nu\tau\alpha\rho_1$ ’—everything flows? *J. Nonnewton. Fluid Mech.* **81**, 133–178 (1999)
9. Hotten, B.W.: Optical studies of lubricating grease structure. *NLGI Spokesm.* **19**(1), 14 (1955)
10. Yuxin, Z., Bosman, R., Lugt, P.M.: A model for shear degradation of lithium soap grease at ambient temperature. *Tribol. Trans.* (2016). doi:[10.1080/10402004.2016.1272730](https://doi.org/10.1080/10402004.2016.1272730)
11. Barnes, H.A.: Thixotropy: a review. *J. Nonnewton. Fluid Mech.* **70**, 1–33 (1997)
12. Paszkowski, M.: Assessment of the effect of temperature, shear rate and thickener content on the thixotropy of lithium lubricating greases. *Proc. Inst. Mech. Eng. J J. Eng. Tribol.* **227**, 209–219 (2013)
13. Czarny, R.: The influence of surface material and topography on the wall effect of grease. *Lubr. Sci.* **14**, 255–274 (2004)
14. Czarny, R., Moes, H.: Some aspects of lubricating grease flow. In: *Proceedings of the 3rd International Conference on Tribology Eurotrib*, vol. 8, pp. 68–85. (1981)
15. Vinogradov, G.W., Froishteter, G.B., Trillski, K.K.: The generalised theory of flow of plastic disperse systems with account of the wall effect. *Rheol. Acta* **17**, 156–165 (1978)
16. Bramhall, A.D., Hutton, J.F.: Wall effect in the flow of lubricating grease in plunger viscosimeters. *Br. J. Appl. Phys.* **11**, 363–369 (1960)
17. Kosasih, P.B., Tieu, A.K., Li, E.B.: PIV study of lubricant flow in journal bearing supply pocket. In: *Proceedings of the 14th Australasian Fluid Mechanics Conference*, pp. 481–484, Adelaide University, Adelaide, Australia, 10–14 December 2001
18. Sarkar, C., Westerberg, L.G., Höglund, E., Lundström, T.S.: Numerical simulations of lubricating grease flow in a rectangular channel with- and without restrictions. *Tribol. Trans.* (2017). doi:[10.1080/10402004.2017.1285090](https://doi.org/10.1080/10402004.2017.1285090)
19. Baart, P., Green, T.M., Li, J.X., Lundström, T.S., Westerberg, L.G., Höglund, E., Lugt, P.M.: The influence of speed, grease



- type, and temperature on radial contaminant particle migration in a double restriction seal. *Tribol. Trans.* **54**, 867–877 (2011)
20. COMSOL Multiphysics® v. 5.2. <http://www.comsol.com>. COMSOL AB, Stockholm, Sweden. Accessed May 15 2016
  21. Mitsoulw, E., Abdali, S.S.: Flow simulation of Herschel–Bulkley fluids through extrusion dies. *Can. J. Chem. Eng.* **71**, 147–160 (1993)
  22. Li, J.: Lubricating grease experiments and modelling of wall-bounded and free-surface flows. Doctoral thesis, Lulea University of Technology, Lulea (2014)